

A novel magnetically levitated tip/tilt motion platform

E. Csencsics* G. Doblinger* and G. Schitter*

* Automation and Control Institute, TU Wien, Vienna, Austria
(e-mail: csencsics@acin.tuwien.ac.at).

Abstract:

This paper presents the mechatronic system design and control of a tip/tilt motion platform with a magnetically levitated mover tailored for dynamic rotational scanning operation. It employs a Lorentz force-based actuation system with five degrees of freedom and four spherical Halbach arrays on a fully passive mover. The system includes highly integrated optical proximity sensors for sensing the mover position in all degrees of freedom and a passive magnetic bearing for restraining the non-actuated degree of freedom. The actuation system enables a mechanical angular range of $\pm 1^\circ$ in both axes, with first structural modes of the 3D printed mover occurring at 1 kHz. A control system is designed for the five actively controlled degrees of freedom for obtaining a robustly stable and precise motion system. The resulting closed-loop system has a bandwidth of 200 Hz in the rotational and 100 Hz in the translational degrees of freedom and a small positioning uncertainty of 0.02% of the full motion range.

Keywords: Mechatronics, Magnetic levitation, System analysis and design, Motion control, Lorentz force actuation

1. INTRODUCTION

Modern magnetically levitated positioning stages mostly offer six degrees of freedom (DoFs) with a rigid moving part and therefore simple mechanics, enabling excitation of forces without physical connection between stator and mover [Zhu et al. (2017)]. Various applications are found in many different industry sectors, such as in lithography machines [Kim and Trumper (1998)]. Levitating planar motors are used as high precision and fast response positioning platforms, working even in demanding environments like vacuum [Zhang et al. (2015)]. In comparison to direct-driven linear motors, friction-losses, the use of lubricants and wear can be avoided, when using fully levitated movers [Nguyen and Kim (2017)]. Other fields of application are active vibration isolation systems for laboratory based and inline precision measurement systems [Kim et al. (2009)][Wertjanz et al. (2022)]. A common property of most levitation stages is the aim for large translational ranges, with the actuation of the rotational DoFs being only a necessity in order to stabilize them, thus resulting in rather small ranges.

Fast steering mirrors (FSMs) [Hedding and Lewis (1990)], also termed tip/tilt mirrors, are opto-mechatronic devices that enable tip and tilt motion of a mirror for optical pointing and scanning applications in various scientific and commercial systems. Applications for pointing operations include beam stabilization in optical systems [Kluk et al. (2012)], tracking of objects and acquisition of optical signals [Guelman et al. (2004)], image stabilization in stare imaging systems [Sun et al. (2015)] and adaptive optics in telescopes [Janssen et al. (2010)]. Applications requiring good scanning properties range from scanning laser sensors [Schlarp et al. (2018)] over scanning optical lithog-

raphy [Zhou Q., et al. (2008)] to confocal microscopy [Yoo et al. (2014)] and material processing [Hedding and Lewis (1990)]. While being mostly actuated by piezo [Csencsics et al. (2020)] or electromagnetic actuators [Csencsics et al. (2019)], particularly beam pointing and staring applications can also benefit from a fully levitated mirror in terms of vibration decoupling, additional translational DoFs and a potentially extended range of rotational motion. At the same time a simple mechanical design is desirable to still enable high system performance in terms of motion range and positioning bandwidth.

This paper presents the mechatronic system design and control of a novel tip/tilt motion platform with magnetically levitated mover for a fast steering mirror system, which comprises an actuation structure with five degrees of freedom and spherically shaped Halbach magnet arrays. Section 2 describes the system design and elaborates on the design choices, while Section 3 deals with components and the system implementation. The system identification and analysis is shown in Section 4, followed by the model-based controller design in Section 5. Section 6 evaluates the system performance and Section 7 concludes the paper.

2. TIP/TILT PLATFORM DESIGN

2.1 System Overview

With focus on rotational tip and tilt motion and the aim of mounting a scanning mirror, a circular system geometry is chosen, resulting in a hemispherical shape of the actuation system. A fully levitated mover would require an actuation of six DoFs. However, for a scanning mirror the in-plane rotation is not critical, as it has no influence on the direction of a reflected beam. For this

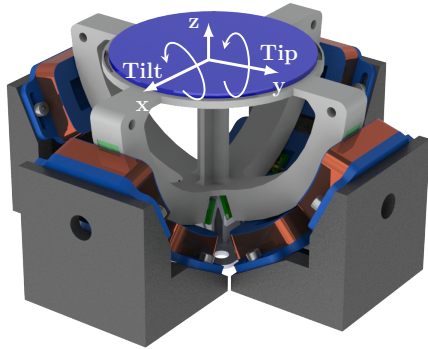


Fig. 1. Tip/tilt platform design showing the floating mover with the introduced coordinate system together with the stator carrying 8 actuation coils.

reason, the tip/tilt motion platform design is reduced to five actuated DoFs, with the handling of the non-actuated DoF discussed in Section 3. Considering typical FSM specifications, a mechanical angular motion range of $\pm 1^\circ$, a bandwidth larger than 100 Hz and a mirror size of 2 inch are targeted, together with a translational motion range of ± 0.1 mm. In Fig. 1 an overview of the system is shown together with the used coordinate system that defines the lateral (x/y) and levitation (z) directions of the floating mover as well as its rotational DoFs. To enable a fully levitated mover without mechanical connection to the stator, Lorentz force actuators are designed. To generate sufficient force for gravity compensation and levitating a floating mover without the need for excessively large currents, the levitation force is distributed over four actuators with individual coils. Actuation of the rotational DoFs is achieved by one coil-pair for each rotation axis, which are chosen for the sake of a balanced actuation, to increase the dynamic range of rotation and to reduce the required driving currents. This results in a total of eight individual actuators as shown in Fig. 1.

2.2 Actuation System

For levitation systems major goals are (i) to keep the mass of the moving parts as small as possible and (ii) to avoid electrical connections to the moving part in order to avoid additional stiffness and a potential limitation of the system range. A way to generate high forces without the need for ferromagnetic yoke parts on the mover, which would increase the mover mass, are Halbach arrays [Halbach (1985)]. A design tradeoff of such a circular array is found in the fact that smaller magnets would lead to a better approximation of a spherical magnetic field, but would also decrease the arrays spatial period. As the spatial period is strongly related to the size of homogeneous magnetic field utilized for force generation, a decrease of it would result in a decreased tip and tilt range of the system. This range limitation can be overcome by electronic commutation [Zhu et al. (2017)], which, however, requires a more complex system control and coil structure. In order to keep coil geometries simple

and decrease the overall system complexity, the range maximization of a non-commutating system is another major design goal. Considering the targeted range and attachable mirror size, ten millimeter magnet cubes are chosen based on an optimization approach.

Two circular-shaped Halbach arrays are used per axis together with four coils for generating translational and rotational forces, as depicted in Fig. 2(a). Two tilted coils (bottom) are used for levitation, trading off a slight decrease in the levitation force for an additional force component enabling the lateral actuation and thus stabilization of the mover.

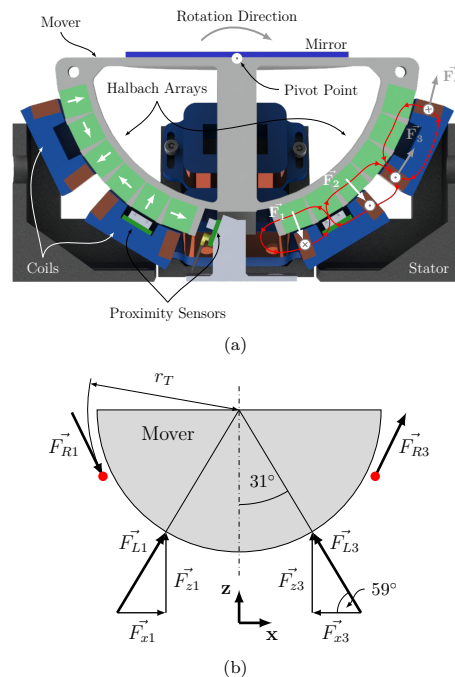


Fig. 2. Actuation system. (a) Sectional view of levitating actuator with indicated magnetic field and the resulting forces for levitation and rotation. F_1 and F_2 denote the levitation force, F_3 and F_4 the rotational force. (b) Force vectors for x- and z-axes generated by the levitation coils L_1 and L_3 with the torque generating forces F_{R1} and F_{R3} .

For generating the torque required for rotational actuation, one additional coil is placed at each side of the mover. In the left half of the mover in Fig. 2(a) the magnetization directions of the Halbach array are depicted. The right half shows the simplified magnetic field generated by the Halbach array. Considering the geometries and directions of Lorentz force actuation, the torque coils are placed in radially oriented parts of the magnetic field, while the levitation coils are placed in tangentially oriented parts. Exemplary current directions inside the coils are shown together with the resulting Lorentz forces in the coil centers. The forces F_1 and F_2 generate the levitation force and control the length of the air gap, which is designed

to be 0.5 mm for nominal operation. By maintaining a targeted levitation height, a well defined pivot point on top of the hemispherical mover is obtained. \mathbf{F}_3 and \mathbf{F}_4 are used to generate the torque for rotational motion. For a balanced system design and for increasing the applicable torque, two coils with opposing current directions are used per rotation axis.

For maximizing the applied forces, the magnetic flux density B , the number of turns per coil N , the current I and the wire length l exposed to B are the determining parameters. The resulting magnetic flux density is defined by the magnet configuration and mostly limited by weight limitations. The limiting factor in terms of coil turns and current is the maximum current and heat dissipation. The remaining parameter is the effective wire length, which is determined via the magnets' width. Considering the individual forces to act on the respective coil center, a homogeneous magnetic flux density and perpendicular current and flux directions, the levitation force is calculated via

$$\mathbf{F}_z = \mathbf{F}_{z1} + \mathbf{F}_{z2} + \mathbf{F}_{z3} + \mathbf{F}_{z4} = 4 \cdot I_l \cdot k_A \cdot \sin(59^\circ) \cdot \mathbf{e}_z, \quad (1)$$

with the motor constant $k_A = NBl$ and the geometric relations from Fig. 2(b), which depicts the projection of the resulting vertical force for two of the four levitation coils. The levitation force is generated by levitation currents I_l through all four levitation coils ($L1-L4$, see Fig. 4(a)) and therefore the sum of four generated forces in z-direction. For translational positioning in x- and y-direction, two levitation coils are driven differentially by I_x and I_y which are superimposed to the levitation current in the levitation coils with alternating sign and lead to the lateral forces

$$\mathbf{F}_x = \mathbf{F}_{x1} - \mathbf{F}_{x3} = 2 \cdot I_x \cdot k_A \cdot \cos(59^\circ) \cdot \mathbf{e}_x \quad (2)$$

$$\mathbf{F}_y = \mathbf{F}_{y2} - \mathbf{F}_{y4} = 2 \cdot I_y \cdot k_A \cdot \cos(59^\circ) \cdot \mathbf{e}_y \quad (3)$$

calculated by the projection of the generated forces in the lateral axes. For torque calculation, the force lever is defined by r_T , which is the distance from the pivot point to the torque coil ($R1-R4$) center, yielding the torques

$$\mathbf{T}_{Tip} = (\mathbf{F}_{R1} + \mathbf{F}_{R3}) \cdot r_T = 2 \cdot I \cdot k_A \cdot r_T \cdot \mathbf{e}_{Tip} \quad (4)$$

$$\mathbf{T}_{Tit} = (\mathbf{F}_{R2} + \mathbf{F}_{R4}) \cdot r_T = 2 \cdot I \cdot k_A \cdot r_T \cdot \mathbf{e}_{Tit}. \quad (5)$$

2.3 Sensing System

According to Earnshaw's theorem [Earnshaw (1842)], feedback operation is essential for stable operation of levitating systems. This sets the requirement for displacement sensing in every controllable DoF. Due to the symmetric design and the use of two levitation coils per axis, an air gap measurement is implemented for each levitation coil, leading to six sensors in total. The sensors for air gap length measurements are placed inside the four levitation coils. Rotational motion sensing is achieved by tangential displacement measurement at the radius r_S (see Fig. 2(a)). The sensor positions are chosen to ensure observability by concurrent distance measurement and force direction. Custom-made optical proximity sensors with a bandwidth of 10 kHz and a range of 4 mm are employed for reasons of size, range and adequate resolution. With the compact size of this sensor, it is possible to integrate all sensors into the stator without major design limitations.

By the co-location of sensor and actuator, the same geometric relations as for the force generation are applicable.

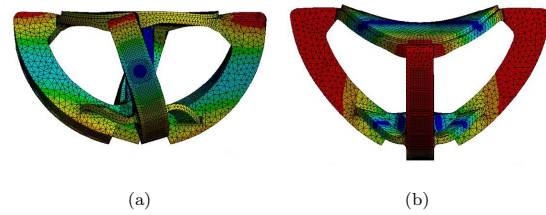


Fig. 3. First two structural modes of the designed mover at (a) 943 Hz and (b) 953 Hz.

Using all four air gap distance measurements (d_{L1} to d_{L4}) the levitation height

$$d_z = \frac{d_{L1} + d_{L2} + d_{L3} + d_{L4}}{4} \cdot \sin(59^\circ) \quad (6)$$

is obtained by the mean of all four distance values projected onto the z-axis.

For calculating the lateral displacement in x- and y-direction, differential distance measurements and an according projection is used, resulting to

$$d_x = (d_{L1} - d_{L3}) \cdot \cos(59^\circ)/2 \quad (7)$$

$$d_y = (d_{L2} - d_{L4}) \cdot \cos(59^\circ)/2. \quad (8)$$

With the use of the sensor placement radius r_S and the tangential measurements (d_{Tip} and d_{Tit}), the angles

$$\varphi_{Tip} = \text{atan}\left(\frac{d_{Tip}}{r_S}\right) \approx \frac{d_{Tip}}{r_S} \quad (9)$$

$$\varphi_{Tit} = \text{atan}\left(\frac{d_{Tit}}{r_S}\right) \approx \frac{d_{Tit}}{r_S} \quad (10)$$

are obtained, with the small angle approximation being applicable for the targeted system range of $\pm 1^\circ$ (maximum error of 0.1 mdeg). This coordinate transformation enables centered alignment of the mover as well as a fixed levitation height.

3. SYSTEM SETUP

The floating mover is the only moving part of the tip/tilt motion platform design. Due to this fact the design is made with respect to mechanical stiffness, while still keeping the weight as low as possible. With six magnetic cubes used per Halbach array and four implemented arrays, a total of 24 magnets are used to form the required magnetic configuration. Using magnet cubes (N42 grade neodymium) with an edge length of 10 mm, a mover radius of 65.5 mm is obtained. Due to the size of the mover, an 80 mm mirror is attached on top (see Fig. 4(b)). In order to avoid low frequency structural trampoline modes of the mirror plane, a supporting center post is integrated into the mover. The mover is manufactured via 3D printing with lightweight and stiff acrylonitrile butadiene styrene (ABS), resulting in an overall mover mass of 277 g (inertia 309 564 gmm²). A modal analysis of the mover (Ansys, Canonsburg, USA) reveals its first two structural mode shapes, which are depicted in Fig. 3. Since the related resonance frequencies are almost at 1 kHz, they are located well above the targeted system bandwidth. A magneto-static simulation is conducted for estimating the mean magnetic flux densities, which result in $B_1 = 85$ mT for the levitation and $B_2 = 159$ mT for the rotation coils.

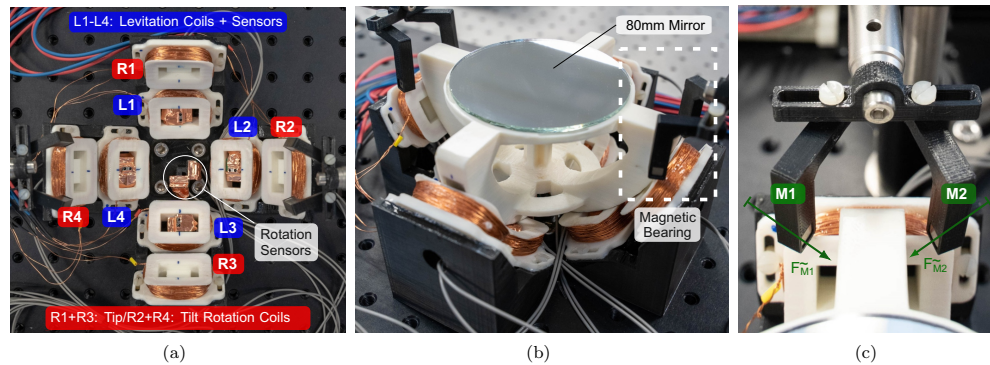


Fig. 4. Experimental setup. (a) Five DoF stator with coil configuration. (b) Assembled setup with levitated mirror mover. (c) Magnetic bearing with two magnet cubes ($M1$ and $M2$) centering the mover with repulsive magnetic force in the non-actuated degree of freedom.

For the stator construction ferromagnetic materials need to be avoided to eliminate reluctance forces from affecting the mover and degrading the system performance. As a consequence, the stator frame is also built from 3D printed components mounted on an aluminium basis. Figure 4(a) shows a top view of the stator with the levitation coils ($L1-L4$) and the torque coils ($R1-R4$). Due to the limited coil cross section, the coils are made from 0.4 mm wire with 150 windings per coil ($l = 25$ mm) and are driven via custom made PI-controlled current amplifiers with 10 kHz bandwidth. The low resistance of the manufactured coil (2.2Ω) represents a high load for the amplifiers, such that additional power resistors are connected in series to stay within the safe operating area. For driving the rotational actuator $R1$ and $R4$ are connected in series for tip-, $R2$ and $R3$ for tilt-actuation. All levitation coils are driven individually due to the higher current demands and to be able to compensate for alignment or variations of the magnetic field. The six proximity sensors are visible inside the levitation coils and in the stator center. As dynamic current changes influence the sensor readout due to induction, copper shielding tape is used to connect the sensor heads to ground and suppress this influence.

As discussed earlier, the rotational DoF around the vertical axis remains non-actuated in the proposed system design. For restricting the rotation in order to maintain good alignment between stator and mover, a passive magnetic bearing is implemented. As illustrated in Fig. 4(c), the repulsive force of two magnetic cubes ($M1$ and $M2$) acting on the stray field generated by the Halbach-array is used to center the mover over the coil axes.

4. SYSTEM IDENTIFICATION AND ANALYSIS

For identifying the dynamics of the prototype system, a system analyzer (3562A, Hewlett-Packard, Palo Alto, CA, USA) is used. The inputs of the current amplifiers and the displacements in the respective DoFs are considered as system inputs and outputs, respectively. As the levitated tip/tilt mirror system is inherently unstable, a closed-loop identification procedure is required. Simple double integrator (mass line) models are derived based on the simulated motor constants, the sensor gains and the obtained

values for the mover mass and its inertia. Based on these models, robust PID controllers are designed for a crossover frequency of $f_c = 50$ Hz [Csencsics and Schitter (2017)]. The frequency response of the respective system axis $G(s)$ is then obtained by dividing the measured complementary sensitivity $T(s) = G(s)C(s)/(1 + G(s)C(s))$ by the measured input sensitivity function $U(s) = C(s)/(1 + G(s)C(s))$.

Figure 5(a) illustrates this procedure for the vertical z -axis. The plant dynamics $G_z(s)$ in Fig. 5(a) show good agreement of the simplified mass line model $G_{sim,z}(s)$. For also considering the actual residual stiffness and damping, the simplified system model is modified with a fitted stiffness of $k_z = 200$ mNm $^{-1}$ and a low damping of $d_z = 831$ μ Nsm $^{-1}$. The stiffness is introduced by the z -distance dependency of the magnetic field generated by the Halbach arrays. However, with the targeted bandwidth significantly higher than the resulting resonance frequency, this change in stiffness is no issue for system operation. At around 600 Hz a right half plane zero (RHZ) is observed, which entails a significant phase drop and represents a bandwidth limiting factor for the system. The RHZ may be explained by the limited mechanical stiffness of the stator or slightly deviating gains in the amplifiers of the levitation coils. After the RHZ a left half plane pole (LHP) occurs at about 1 kHz, which matches the obtained structural modes (see Fig. 3) well. Above 1 kHz the system noise floor is reached at around -40 dB. To model the occurring resonances in $G_{mod,z}(s)$, pole and zero pairs are fitted and the delay of the rapid prototyping system is considered.

The dynamics of the x - and y -axis yield similar results with slightly varying stiffness at frequencies below 5 Hz, which are caused by the passive magnetic bearing for maintaining alignment (see Fig. 4(c)) but are again not critical for feedback control. In both translational axes the same combination of RHZ and LHP as for the vertical axis is observed, with the RHZ occurring already at 263 Hz and 316 Hz for the x - and y -axis (data not shown).

In Fig. 5(b) the frequency responses of the tip and tilt axis are depicted, both again showing good agreement with the simplified inertia model. The inherent open loop unstable

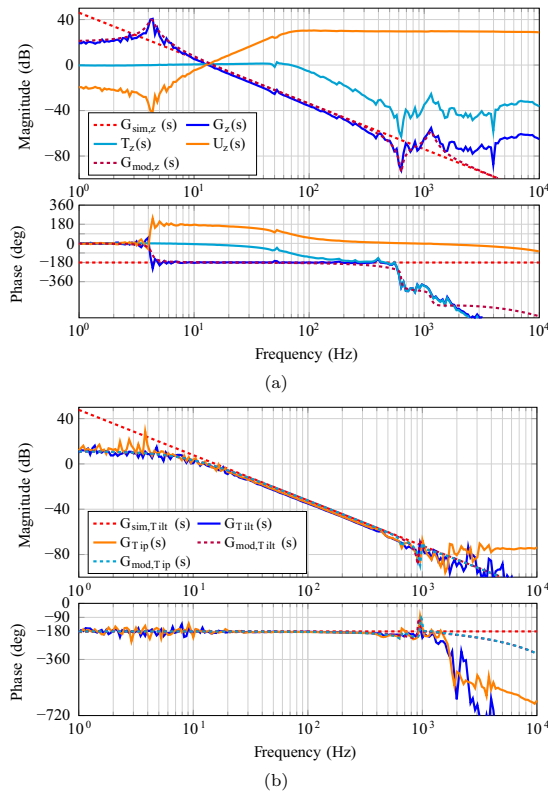


Fig. 5. System identification. (a) Bode plot of z -axis dynamics $G_z(s)$ calculated from the ratio of $T_z(s)$ and $U_z(s)$. Additionally the simplified $G_{sim,z}(s)$ and adapted $G_{mod,z}(s)$ axis models are shown. (b) Bode plot of tip- and tilt-axis dynamics ($G_{Tip}(s)$ and $G_{Tilt}(s)$) together with the simplified ($G_{sim,Tip}(s) = G_{sim,Tilt}(s)$) and modified axis models ($G_{mod,Tip}(s)$ and $G_{mod,Tilt}(s)$).

dynamics are observable with a resulting negative stiffness of -50 mNm and a phase of -180° at low frequencies. The symmetric construction results in comparable dynamics for both axes, without major impact from the magnetic bearing. The first structural mode occurs at about 1 kHz, in good agreement with the modal analysis of the mover shown in Fig. 3. This fact would enable a considerably higher control bandwidth than for the translational DoFs. Crosstalk measurements reveal that the crosstalk between the individual DoFs is between 20 and 40 dB lower than the gain in the individual axis responses (data not shown), justifying single-input-single-output controllers for each DoF.

5. CONTROLLER DESIGN AND IMPLEMENTATION

The design of the feedback controller is done with the aim of maximizing the closed-loop system bandwidth for a high system performance based on the obtained plant models. As seen in the system identification for the lateral DoFs, the main bandwidth limiting factor is the occurring

Table 1. PID control parameters for all DoFs.

DoF	k_p	k_i	k_d	PM[$^\circ$]	GM [dB]
x	13.7	478	0.12	60.7	18.4
y	13.7	478	0.13	50.2	18.8
z	4.14	144	0.04	50.8	23
Tip	30.9	3236	0.098	48.1	17.7
Tilt	30.8	3230	0.098	49.1	18

right half plane zero. For the rotational DoFs there is no limiting factor until the structural mode around 1 kHz. However, the translational DoFs are needed to maintain a well-defined pivot point for rotation. Given the low but still existing coupling between the individual DoFs, high frequency rotational motions would disturb the pivot point location, degrading the entire optical performance. For this reason, the entire system performance is determined by the slowest plant, which is the x -axis with a RHZ at 263 Hz. Nevertheless, the crossover frequency of the rotational axes can be slightly higher to increase the tracking performance also for lower frequencies. Therefore the crossover frequencies are chosen to be 50 Hz for the translational and 150 Hz for the rotational DoFs to obtain a robustly stable system with phase margins around 50° . Using Alpha tuning [Csencsics and Schitter (2017)] with a parameter $\alpha = 3$ as a good compromise between performance and robustness, tamed PID controllers of the form

$$C_{PID}(s) = k_p + \frac{k_i}{s} + k_d s \frac{1}{\frac{s}{\alpha\omega_c} + 1} \quad (11)$$

$$k_p = \frac{1}{\alpha |G(s)|_{s=j\omega_c}} \quad (12)$$

$$k_i = k_p \frac{\omega_c}{\alpha^2} \quad (13)$$

$$k_d = k_p \frac{\alpha}{\omega_c} \quad (14)$$

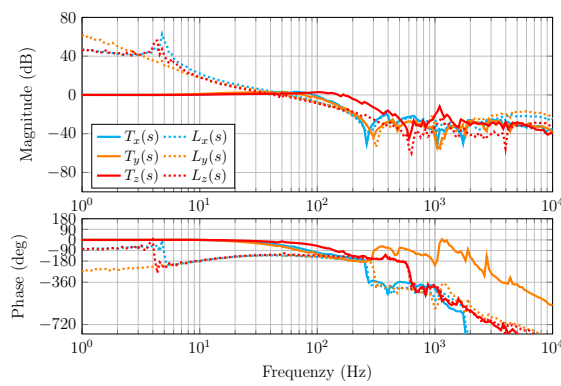
are obtained for the individual axes. Table 1 lists the implemented PID parameters together with the obtained phase (PM) and gain margins (GM). To attenuate the structural mode around 1.1 kHz in the translational DoFs, the PID controllers in these DoFs are cascaded with an additional notch filter at this frequency.

For system operation and controller implementation, a rapid prototyping system (MicroLabBox, dSpace, Paderborn, Germany) with a sampling frequency of 40 kHz is used. The poles and zeros are directly transformed to the discrete time domain by using the relation $z = e^{s/f_s}$ to guarantee that the notch filters are located exactly at the desired frequencies [Franklin et al. (1997)]. In Fig. 6(a) and (b) the measured loop gains of all translational and rotational DoFs are depicted, respectively.

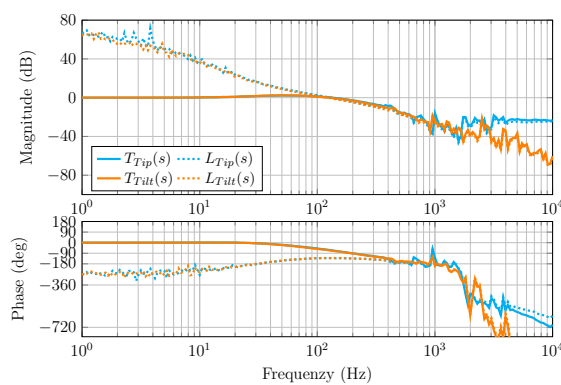
6. EVALUATION OF SYSTEM PERFORMANCE

For evaluation of the system, the closed-loop dynamics, the operational range, the tracking performance, and the positioning uncertainty are investigated.

The measured complementary sensitivity functions of the tip/tilt platform system with the designed PID controllers are shown in Fig. 6(a) and (b) for the translational and rotational DoFs, respectively. In the lateral DoFs -3 dB bandwidths of 100 Hz are obtained, while the vertical DoF shows a bandwidth of 190 Hz, which is explained by a



(a)



(b)

Fig. 6. Measured complementary sensitivity functions and loop gains for (a) the translational DoFs x, y and z, and (b) the rotational tip and tilt DoFs.

higher phase margin of the loop gain. Both rotational DoFs result in a bandwidth of 200 Hz. Due to the relatively large phase margins, essentially no peaking is observable in the magnitude responses.

The operational range in the individual DoFs at the nominal air gap length of 0.5 mm results in ± 0.2 mm in the lateral directions and $\pm 1^\circ$ in tip and tilt. The limiting factor for the rotational range is currently the optical sensing system, as up to $\pm 2.5^\circ$ would be possible with the designed actuation system. In Fig. 7 the performance of the system while accurately tracking a full scale raster ($f_{tip} = 10$ Hz and $f_{tilt} = 0.5$ Hz) and Lissajous trajectory ($f_{tip} = 3$ Hz and $f_{tilt} = 4$ Hz) is shown. The slight S-shaped tendency, which is barely observable in the internal sensor space but more pronounced in the projected images, is caused by rotational motion in the non-actuated DoF.

The resulting positioning uncertainty of the tip/tilt platform system is determined at constant references applied to all DoFs. The lateral x- and y-axis show a positioning uncertainty of about 300 nm, while the z-axis shows an uncertainty of only 146 nm, which is a factor of 2 smaller and explained by averaging four distance signals. The rotational positioning uncertainty of the tip and tilt axis

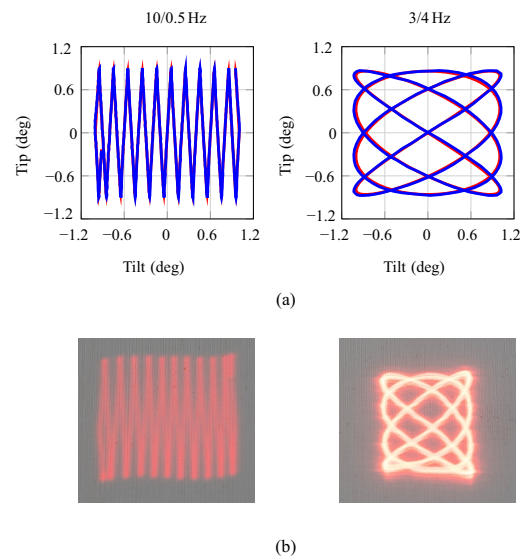


Fig. 7. Two dimensional scanning motion. (a) Raster and Lissajous trajectories with reference (red) and position sensor signal (blue). (b) Photograph with long term exposure of deflected laser beam in experimental projection system.

result both in about $390 \mu\text{deg}$ rms ($6.8 \mu\text{rad}$ rms), which is 0.02% of the full scale range.

In summary, it is successfully demonstrated that the proposed tip/tilt motion platform for a beam steering mirror system provides a fully levitated mover with a mechanical angular range of $\pm 1^\circ$, achieves a bandwidth of 200 Hz and shows good tracking performance and low positioning uncertainty.

7. CONCLUSION

This paper presents a novel tip/tilt motion platform system design with a fully levitated mover tailored for dynamic scanning operation. The design is centered around a Lorentz force-based actuation system with five degrees of freedom and four spherical Halbach arrays on the fully passive mover. It provides a mechanical angular range of $\pm 1^\circ$ in both axes, with first structural modes of the mover occurring at around 1 kHz. After a detailed system description and analysis, including the dynamics of and the crosstalk between the individual DoFs, model-based PID controllers, partially cascaded by notch filters, are designed to obtain a robustly stable closed-loop system. The resulting closed-loop system has a bandwidth of 200 Hz in the rotational DoFs and a small positioning uncertainty of 0.02% of the full scale range.

Future work is concerned with enhancing the rotational range of the system, extending the actuation structure to the remaining rotational DoF as well as with compacting the entire system design.

REFERENCES

- Csencsics, E. and Schitter, G. (2017). Parametric PID controller tuning for a fast steering mirror. *IEEE Conference on Control Technology and Applications (CTA)*, 1673–1678.
- Csencsics, E., Schlarp, J., Schopf, T., and Schitter, G. (2019). Compact high performance hybrid reluctance actuated fast steering mirror system. *Mechatronics*, 62, 102251.
- Csencsics, E., Sitz, B., and Schitter, G. (2020). Integration of control design and system operation of a high performance piezo actuated fast steering mirror. *IEEE Transactions on Mechatronics*, 25(1), 239–247.
- Earnshaw, S. (1842). On the nature of the molecular forces which regulate the constitution of the luminiferous ether. *Trans. Camb. Phil. Soc.*, 7, 97–112.
- Franklin, G.F., Powell, D.J., and Workman, M.L. (1997). *Digital Control of Dynamic Systems*. Prentice Hall.
- Guelman, M., Kogan, A., Livne, A., Orenstein, M., and Michalik, H. (2004). Acquisition and pointing control for inter-satellite laser communications. *IEEE Transactions on Aerospace and Electronic Systems*, 40(4), 1239.
- Halbach, K. (1985). Application of permanent magnets in accelerators and electron storage rings. *Journal of Applied Physics*, 57(8), 3605–3608.
- Hedding, L.R. and Lewis, R.A. (1990). Fast steering mirror design and performance for stabilization and single axis scanning. *SPIE 340*, 1304, 14–24.
- Janssen, H., Teuwen, M., Navarro, R., Tromp, N., Elswijk, E., and Hanenburg, H. (2010). Design and prototype performance of an innovative cryogenic tip-tilt mirror. *Modern Technologies in Space and Ground-based Telescopes, Proceedings of the SPIE*, 77394A.
- Kim, W.J. and Trumper, D.L. (1998). High-precision magnetic levitation stage for photolithography. *Precision Engineering*, 22(2), 66–77.
- Kim, Y., Kim, S., and Park, K. (2009). Magnetic force driven six degree-of-freedom active vibration isolation system using a phase compensated velocity sensor. *Review of Scientific Instruments*, 80(4).
- Kluk, D.J., Boulet, M.T., and Trumper, D.L. (2012). A high-bandwidth, high-precision, two-axis steering mirror with moving iron actuator. *Mechatronics*, 22(3), 257.
- Nguyen, V.H. and Kim, W.J. (2017). Two-phase lorentz coils and linear halbach array for multiaxis precision-positioning stages with magnetic levitation. *IEEE/ASME TMECH*, 22(6), 2662–2672.
- Schlarp, J., Csencsics, E., and Schitter, G. (2018). Optical scanning of laser line sensors for 3d imaging. *Applied Optics*, 57(18), 5242–5248.
- Sun, C., Ding, Y., Wang, D., and Tian, D. (2015). Backscanning step and stare imaging system with high frame rate and wide coverage. *Applied Optics*, 54(16), 4960–4965.
- Wertjanz, D., Csencsics, E., Kern, T., and Schitter, G. (2022). Bringing the lab to the fab: Robot-based inline measurement system for precise 3d surface inspection in vibrational environments. *IEEE TIE*, 69(10), 10666–10673.
- Yoo, H., van Royen, M.E., van Cappellen, W.A., Houtsmuller, A.B., Verhaegen, M., and Schitter, G. (2014). Automated spherical aberration correction in scanning confocal microscopy. *Review of Scientific Instruments*, 85, 123706.
- Zhang, L., Kou, B., Xing, F., Jin, Y., Zhang, H., and Zhu, J. (2015). A magnetically levitated synchronous permanent magnet planar motor with concentric structure winding used for lithography machine. *Journal of Applied Physics*, 117(17), 17B525.
- Zhou Q., et al. (2008). Design of fast and steering mirror and systems for precision and laser beams and steering. *IEEE Workshop on Robotic and Sensors Environments*.
- Zhu, H., Teo, T.J., and Pang, C.K. (2017). Design and modeling of a six-degree-of-freedom magnetically levitated positioner using square coils and 1-d halbach arrays. *IEEE TIE*, 64(1), 440–450.